ELSEVIER

Journal of Nuclear Materials 300 (2002) 57–64

journal of nuclear materials

www.elsevier.com/locate/jnucmat

Thermal conductivities of irradiated UO_2 and $(U, Gd)O_2$ pellets

Masaki Amaya [a,*], Mutsumi Hirai [a,1], Hiroshi Sakurai [a], Kenichi Ito [b,2], Masana Sasaki [b,2], Terumitsu Nomata [c,2], Katsuichiro Kamimura [d], Ryo Iwasaki [d,2]

[a] *Nippon Nuclear Fuel Development Co., Ltd., 2163, Narita-cho, Oarai-machi, Higashi-ibaraki-gun, Ibaraki-ken 311 1313, Japan*
[b] *Hitachi Ltd., 1-1, 3-chome, Saiwai-cho, Hitachi-shi, Ibaraki-ken 317 8511, Japan*
[c] *Toshiba Corporation, 8, Shin-sugita-cho, Isogo-ku, Yokohama-shi, Kanagawa-ken 235 8523 Japan*
[d] *Nuclear Power Engineering Corporation, Fujita Kanko Toranomon Bldg. (6F), 17-1, 3-chome, Toranomon, Minato-ku, Tokyo, 105-0001, Japan*

Received 28 May 2001; accepted 26 September 2001

Abstract

Thermal diffusivities of UO_2 and $(U, Gd)O_2$ pellets irradiated in a commercial reactor (maximum burnups: 60 GWd/t for UO_2 and 50 GWd/t for $(U, Gd)O_2$) were measured up to about 2000 K by using a laser flash method. The thermal diffusivities of irradiated UO_2 and $(U, Gd)O_2$ pellets showed hysteresis phenomena: the thermal diffusivities of irradiated pellets began to recover above 750 K and almost completely recovered after annealing above 1400 K. The thermal diffusivities after recovery were close to those of simulated soluble fission products (FPs)-doped UO_2 and $(U, Gd)O_2$ pellets, which corresponded with the recovery behaviors of irradiation defects for UO_2 and $(U, Gd)O_2$ pellets. The thermal conductivities for irradiated UO_2 and $(U, Gd)O_2$ pellets were evaluated from measured thermal diffusivities, specific heat capacities of unirradiated UO_2 pellets and measured sample densities. The difference in relative thermal conductivities between irradiated UO_2 and $(U, Gd)O_2$ pellets tended to become insignificant with increasing burnups of samples.

PACS: 28.41.Bm; 65.40.−b; 61.82.−d; 61–82.Fk

1. Introduction

With increasing burnup of light water reactor (LWR) fuels, it becomes more important to estimate the irradiation behavior of the fuel pellets under high burnup. Thermal conductivity of fuel pellets is one of the most important thermal properties for calculating the fuel temperature during irradiation.

For high-burnup fuels, fission products (FPs) accumulate in fuel pellets. The increased crystal lattice strains caused by irradiation-induced point defects and formation of microbubbles are also observed in irradiated UO_2 pellets [1–3]. Thermal conductivity of fuel pellets is

* Corresponding author. Present address: Global Nuclear Fuel – Japan Co., Ltd., 2163 Narita-cho, Oarai-machi, Higashi-ibaraki-gun Ibaraki-ken, 311 1313, Japan. Tel.: +81-29 267 9011; fax: +81-29 267 9014.
E-mail address: amaya@nfd.co.jp (M. Amaya).
[1] Present address: Global Nuclear Fuel – Japan Co., Ltd., 2163 Narita-cho, Oarai-machi, Higashi-ibaraki-gun, Ibaraki-ken, 311 1313, Japan.
[2] Present address: Global Nuclear Fuel – Japan Co., Ltd., 13-8, Kamiooka Nishi 1-chome, Kounan-ku, Yokohama-shi, Kanagawa-ken, 233 0002, Japan.

0022-3115/02/$ - see front matter
PII: S0022-3115(01)00704-8

affected by these FP impurities and irradiation-induced defects, and it is necessary to evaluate the quantitative changes in the thermal conductivity due to them. It is well known that thermal conductivity of undoped UO_2 pellets decreases with increasing amounts of point defects such as soluble impurities and also with accumulation of defect clusters. Therefore, the thermal conductivity of fuel pellets is expected to degrade with burnup due to the accumulation of FPs and irradiation-induced defects.

The thermal conductivities of stoichiometric UO_2 pellets irradiated in a material test reactor up to about 120 GWd/t (2.8×10^{21} fissions cm^{-3}) have been measured [4–12]. In particular, at temperatures below about 800 K, it was found that the thermal conductivities degraded in comparison with unirradiated UO_2 and simulated FPs-doped UO_2. After the irradiated samples were annealed at temperatures above 1000 K, the thermal diffusivities and thermal conductivities recovered. However, for $(U, Pu)O_2$ irradiated up to burnups of 35 GWd/tM in a fast breeder reactor (FBR) [13,14], the burnup dependence of thermal conductivities and the thermal conductivity recovery were not clearly observed. In addition, there have been few studies on the thermal conductivities of irradiated $(U, Gd)O_2$ pellets, and the effect of gadolinium on the thermal conductivities of irradiated fuel pellets has not been clarified yet.

The thermal conductivity degradation by soluble FPs has already been formulated [15,16], but the effects of crystal lattice strain caused by irradiation-induced point defects and of microbubbles were not sufficiently quantified [17–19]. In this study, the thermal diffusivities of UO_2 and $(U, Gd)O_2$ pellets were measured for base-irradiated samples by using a laser flash method up to 2000 K, and their thermal conductivities were evaluated by using the thermal diffusivities, measured sample densities and specific heat capacities of unirradiated UO_2. The evaluation was carried out to quantify the effects of irradiation-induced defects on thermal conductivities and to explain the thermal conductivity behavior.

2. Experimental

2.1. Sample preparation

Since the fuel pellets irradiated in a commercial reactor generally have many radial cracks (and sometimes circumferential cracks) and high radioactivity, microsamples have advantages of decreasing the crack effects on the thermal diffusivity and of easier sample handling. Therefore, an experimental method for thermal diffusivity measurements was developed previously for small samples [17].

The fuel pellets irradiated in a commercial reactor for 1–5 reactor cycles were sliced into disks of about 1 mm thickness. From the disks, disk shaped or regular prismatic specimens were microsampled at a point between the fuel rim and mid-radius ($0.6 < r/r_0 < 0.9$; r/r_0: relative radius of the pellet) of the slices. Their characteristics are summarized in Table 1. Specimens U-1 and U-2 were samples from the top region of a fuel rod. Their irradiated temperatures were evaluated as about 750 K. Specimens U-3–G-4 were samples near the highest power position for fuel rods. Their irradiation temperatures were evaluated as about 1100 K. Specimens G-1–G-4 were obtained from the fuel rods using pellets of doped gadolinia (Gd_2O_3) of 4.5 wt% (6.4 at.%).

For samples U-2 and U-5, thicknesses after the thermal diffusivity measurements were measured and porosity change was estimated. The theoretical densities and porosities of samples were evaluated by considering the mean atomic mass decrease with burnup. Sample porosities were about 4%.

2.2. Thermal diffusivity measurement

Thermal diffusivities of irradiated samples were measured by using a laser flash method. The apparatus for irradiated samples (type: TC-7000UVH; produced by Sinku-Riko) was shielded by iron and lead and modified to allow operation by a remote control system. Schematic diagrams of the apparatus were shown elsewhere [17]. The sample with sample cell was kept in a vacuum of less than 2×10^{-4} Pa during experiments by using turbo-molecular and oil-rotary pumps. The heat source of the laser flash method was a ruby laser with the maximum energy about 6 J. The laser power used was in the range of about 2.5–3.8 J cm^{-2}. A tungsten mesh heater was used for heating the sample with sample cell. The sample temperature was monitored by a W–5% Re/W–26% Re thermocouple located near the sample holder. Prior to thermal diffusivity measurements, another thermocouple of Pt/Pt–Rh was inserted at the sample position in order to obtain a calibration curve for the temperature deviation due to radiation effect. Sample temperatures during measurements were calibrated by using the calibration curves.

The thermal energy was induced on one side of the sample by shining a ruby laser beam for about 500 μs and the temperature response of the other side was measured by using an In–Sb infrared sensor. A half-time method (Fourier method) [20] was used to analyze the temperature responses. A logarithmic method (Laplace method) [21] was also used to analyze them in order to check the validity of thermal diffusivities.

The thermal conductivities were evaluated by multiplying the thermal diffusivity by the specific heat capacity and the sample density as follows:

Table 1
Characteristics of irradiated UO_2 and $(U, Gd)O_2$ samples

Sample no.	Burnup (GWd/t)	Gd_2O_3 conc. (wt%)	Sample characteristics before experiment			Sample characteristics after experiment		Theoretical density (g cm^{-3})
			Sample shape[a]	Density (g cm^{-3})	Porosity (%)	Density [b] (g cm^{-3})	Porosity[b] (%)	
U-1	8.5	0	1	10.45	4.39	–	–	10.93
U-2	8.5	0	1	10.45	4.39	10.05	8.05	10.93
U-3	39.3	0	2	10.41	3.60	–	–	10.80
U-4	42.7	0	2	10.39	3.68	–	–	10.79
U-5	44.7	0	1	10.28	3.11	9.72	9.88	10.79
U-6	48.8	0	2	10.33	4.04	–	–	10.76
U-7	50.1	0	3	10.32	4.10	–	–	10.76
U-8	53.2	0	3	10.30	4.18	–	–	10.75
U-9	56.0	0	2	10.23	4.74	–	–	10.74
U-10	60.0	0	3	10.26	4.36	–	–	10.73
G-1	43.5	4.5 (6.4 at.%)	2	10.24	3.67	–	–	10.63
G-2	46.5	4.5 (6.4 at.%)	2	10.20	3.95	–	–	10.62
G-3	48.8	4.5 (6.4 at.%)	3	10.19	4.00	–	–	10.61
G-4	50.7	4.5 (6.4 at.%)	3	10.17	4.14	–	–	10.61

[a] (1) Disk shape specimen of 2 mm diameter and 1 mm thickness. (2) Regular prismatic (square) specimen of 2 mm sides and 1 mm thickness. (3) Regular prismatic specimen (square) of 1.5 mm sides and 1 mm thickness.
[b] Value estimated from thickness change during the experiment.

$$\lambda = \alpha C_p \rho, \tag{1}$$

where λ, the thermal conductivity; α, the thermal diffusivity; C_p, the specific heat capacity and ρ, the sample density. The specific heat capacities of irradiated UO_2 and $(U, Gd)O_2$ were assumed to be the same as those of unirradiated undoped UO_2 [22], considering that the difference in the specific heat capacities between undoped UO_2 and simulated soluble FPs-doped UO_2 and $(U, Gd)O_2$ was about 2% even at a simulated burnup of 90 GWd/t [15].

Thermal diffusivity measurements were carried out in the following sequence, based on consideration of prior results of X-ray diffraction and TEM observations by other researchers in our laboratory [1–3].

Run 1 measurement: from room temperature to 1200 K.

Run 2 measurement: from room temperature to 1500 K after Run 1 measurement.

Run 3 measurement: from room temperature to 2000 K after Run 2 measurement.

Some of the high-burnup samples were cracked above 1500 K, and their thermal diffusivities could not be measured above that temperature.

From the thermal diffusivity measurements of unirradiated UO_2 pellets having various sizes, the experimental error of this apparatus was estimated for a microspecimen to be within $\pm 6\%$ in the temperature region from 400 to 2000 K [17].

3. Results

3.1. Thermal diffusivities of irradiated UO_2 and $(U, Gd)O_2$ pellets

The examples of the thermal diffusivities for irradiated UO_2 and $(U, Gd)O_2$ pellets are shown in Figs. 1–4. In these figure, thermal diffusivities of unirradiated UO_2, $(U, Gd)O_2$ and SIMFUEL (SIMulated high-burnup FUEL) pellets [15] are also shown for comparison. Furthermore, dotted line in Fig. 1 shows the calculated values in the case that no irradiation-induced defects recover against temperature and chain line in Fig. 1 the calculated values in the case that irradiation-induced point defects recover against temperature [17].

In Fig. 1, the measured values agree well with the chain line and begin to deviate from the dotted lines in 700–800 K. This shows that the thermal diffusivity (conductivity) begins to recover at about 800 K, mainly because of the irradiation-induced point defects recovery [1].

The thermal diffusivities of irradiated UO_2 and $(U, Gd)O_2$ pellets decrease with increasing burnup at lower temperature.

3.2. Thermal conductivities of irradiated UO_2 and $(U, Gd)O_2$ pellets

The examples of the thermal conductivities for irradiated UO_2 and $(U, Gd)O_2$ pellets are shown in Figs. 5–8.

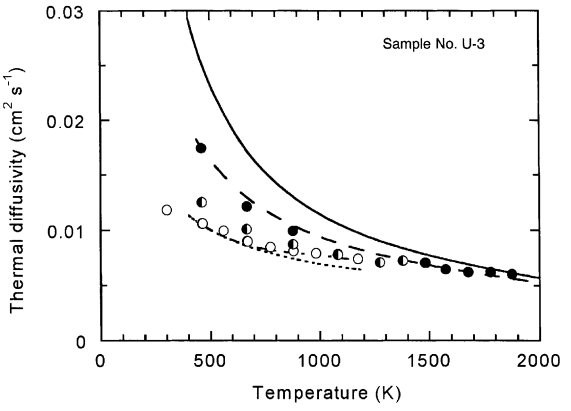

Fig. 1. Thermal diffusivities of U-3 sample. ○, ◐, ●: measured values, ○: RUN 1, ◐: RUN 2, ●: RUN 3; —: unirradiated UO_2 [23]; - - - - -: simulated soluble FPs-doped UO_2 (simulated burnup: 39 GWd/t) [15]; ·····: calculated values assumed that irradiation-induced defects do not recovered against temperature, –·–·–: calculated values assumed that irradiation-induced defects recovered against temperature.

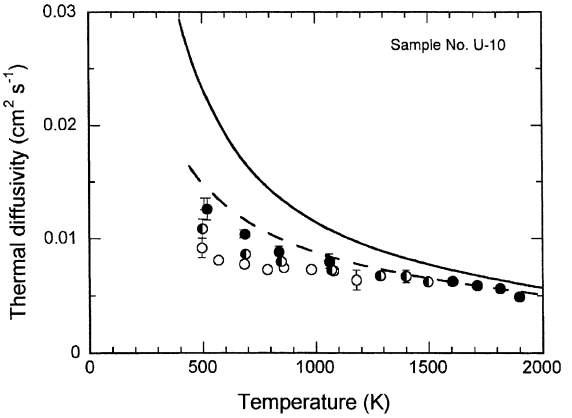

Fig. 2. Thermal diffusivities of U-10 sample. ○, ◐, ●: measured values, ○: RUN 1, ◐: RUN 2, ●: RUN 3; —: unirradiated UO_2 [23]; - - - - -: simulated soluble FPs-doped UO_2 (simulated burnup: 60 GWd/t) [15].

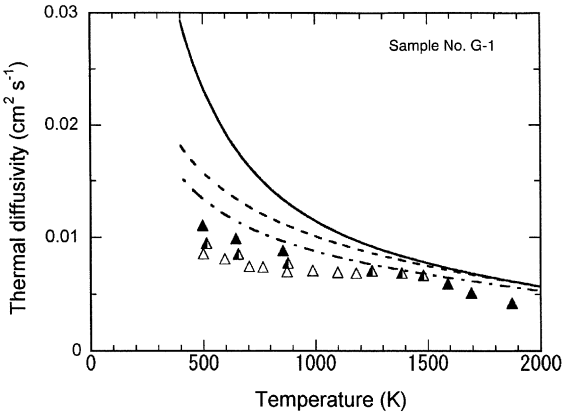

Fig. 3. Thermal diffusivities of G-1 sample. △, ◭, ▲: measured values, △: RUN 1, ◭: RUN 2, ▲: RUN 3; —: unirradiated UO_2 [23]; - - - - -: unirradiated $(U, Gd)O_2$ (Gd_2O_3 concentration: 4.5 wt%) [15]; –·–·–: simulated soluble FPs-doped $(U, Gd)O_2$ (Gd_2O_3 concentration: 4.5 wt%, simulated burnup: 44 GWd/t) [15].

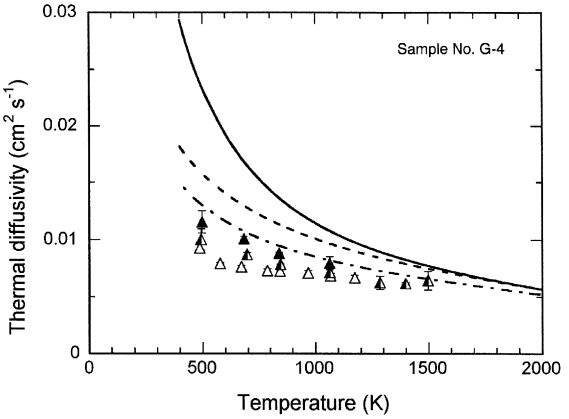

Fig. 4. Thermal diffusivities of G-4 sample. △, ◭, ▲: measured values, △: RUN 1, ◭: RUN 2, ▲: RUN 3; —: unirradiated UO_2 [23]; - - - - -: unirradiated $(U, Gd)O_2$ (Gd_2O_3 concentration: 4.5 wt%) [15]; –·–·–: simulated soluble FPs-doped $(U, Gd)O_2$ (Gd_2O_3 concentration: 4.5 wt%, simulated burnup: 51 GWd/t) [15].

The thermal conductivities of unirradiated UO_2, $(U, Gd)O_2$ and SIMFUEL pellets [15] are also shown for comparison. As shown in these figures, the thermal conductivities of irradiated UO_2 and $(U, Gd)O_2$ samples decreased, compared with those of unirradiated pellets.

Since the thermal conductivity degradation of irradiated UO_2 pellets may be caused by the accumulation of FPs and irradiation-induced defects, the measured thermal conductivities of irradiated pellets were compared with the calculated values in the following section.

4. Discussion

4.1. Thermal conductivities of irradiated UO_2 and $(U, Gd)O_2$ pellets

After ceramic materials such as Al_2O_3, SiC and AlN are irradiated, their thermal conductivities decrease and become close to constant values which are independent of temperature [24,25]. From the discussions using Price's theory [26], it is seen the thermal conductivity

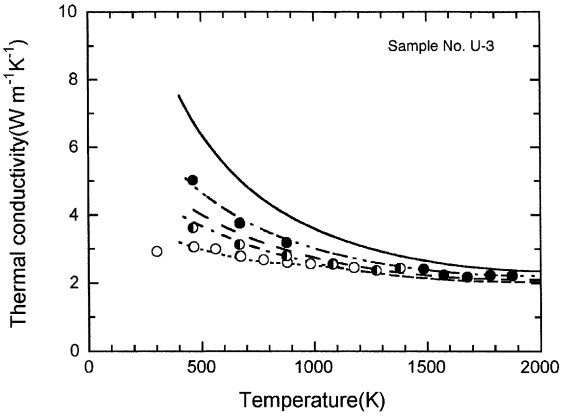

Fig. 5. Thermal conductivities of U-3 sample. ○, ◐, ●: measured values, ○: RUN 1, ◐: RUN 2, ●: RUN 3; ·····, –·–·–, -----: calculated values from Eq. (4); ·····: before point defect recovery; –·–·–: after point defect recovery; -----: after microbubble growth; —: unirradiated UO_2 [15]; —·—·—: simulated soluble FPs-doped UO_2 (simulated burnup: 39 GWd/t) [15].

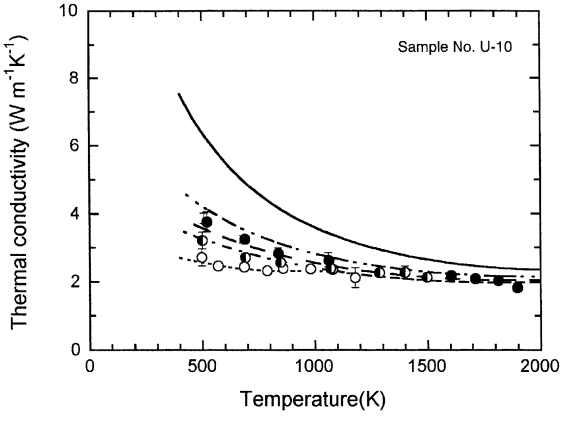

Fig. 6. Thermal conductivities of U-10 sample. ○, ◐, ●: measured values, ○: RUN 1, ◐: RUN 2, ●: RUN 3; ·····, –·–·–, -----: calculated values from Eq. (4); ·····: before point defect recovery; –·–·–: after point defect recovery; -----: after microbubble growth; —: unirradiated UO_2 [15] —·—·—: simulated soluble FPs-doped UO_2 (simulated burnup: 60 GWd/t) [15].

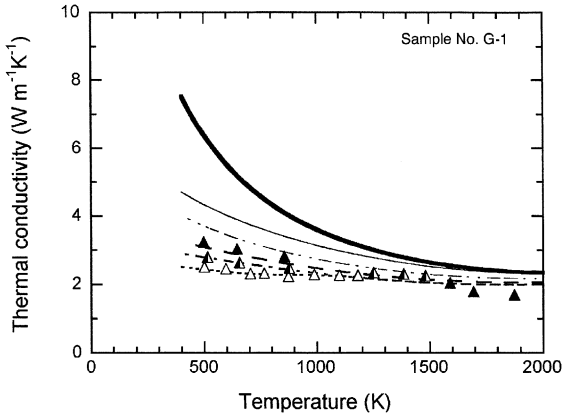

Fig. 7. Thermal conductivities of G-1 sample. △, ◭, ▲: measured values, △: RUN 1, ◭: RUN 2, ▲: RUN 3; ·····, –·–·–, -----: calculated values from Eq. (4); ·····: before point defect recovery; –·–·–: after point defect recovery; -----: after microbubble growth; —: unirradiated UO_2 [15]; – – ·· – – ··-: unirradiated $(U,Gd)O_2$ (Gd_2O_3 concentration: 4.5 wt%) [15]. —·—·—: simulated soluble FPs-doped $(U,Gd)O_2$ (Gd_2O_3 concentration: 4.5 wt%, simulated burnup: 44 GWd/t) [15].

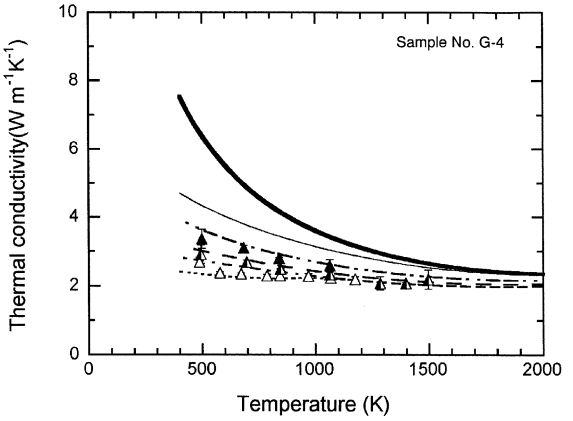

Fig. 8. Thermal conductivities of G-4 sample. △, ◭, ▲: measured values, △: RUN 1, ◭: RUN 2, ▲: RUN 3; ·····, –·–·–, -----: calculated values from Eq. (4); ·····: before point defect recovery; –·–·–: after point defect recovery; -----: after microbubble growth; —: unirradiated UO_2 [15]; —·—·—: unirradiated $(U,Gd)O_2$ (Gd_2O_3 concentration: 4.5 wt%) [15]. —·—·—: simulated soluble FPs-doped $(U,Gd)O_2$ (Gd_2O_3 concentration: 4.5 wt%, simulated burnup: 51 GWd/t) [15].

decreases due to the irradiation-induced impurities, point defects, dislocations and vacancy/interstitial clusters. This fact indicates that it is necessary to consider the effects of irradiation-induced defects on thermal conductivities as well as those of impurities, in order to analyze the thermal conductivity changes of irradiated UO_2 and $(U,Gd)O_2$ pellets.

The temperature ranges for irradiation-defect recovery and microbubble growth in irradiated UO_2, which are based on [1–3], are summarized in Fig. 9. The thermal conductivity changes of irradiated UO_2 and $(U,Gd)O_2$ pellets can be classified as the sum of the effects of irradiation-induced point defects, FPs and irradiation-induced microbubbles.

High concentrations of point defects and extended defects coexist in high-burnup fuel pellets. According to

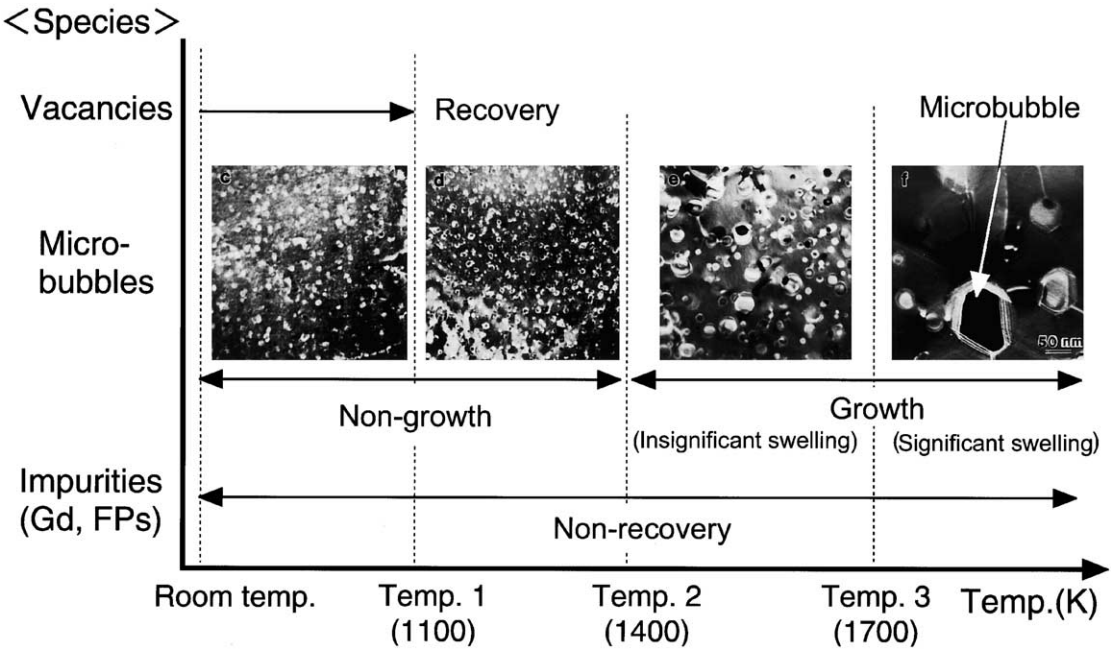

Fig. 9. Temperature ranges for irradiation-induced defect recovery and microbubble growth based on [1–3].

Klemens' theory [27–29], the phonon thermal conductivity of ceramics is expressed as follows using phonon mean free path:

$$\lambda = \frac{1}{3}\int_0^{v_m} [C(v)u(v)l(v)]\,dv, \tag{2}$$

where $C(v)$, the heat capacity of a material per unit volume; $u(v)$, the velocity of a lattice wave; $l(v)$, the phonon mean free path; and v_m, the Debye frequency. The phonon mean free path, $l(v)$, changes due to the phonon scattering mechanism and each contribution to the thermal conductivity in high-burnup fuel pellets is expressed as follows:

$$(1/l(v)) = (1/l_u) + (1/l_p) + (1/l_x), \tag{3}$$

where l_u, the intrinsic mean free path of phonon scattering due to the Umklapp process; l_p, the mean free path of phonon scattering due to point defects; and l_x, the mean free path of phonon scattering due to extended defects.

Substituting Eq. (3) for Eq. (2) leads to the following thermal conductivity formula for high-burnup fuel pellets after considering the lattice vibration frequency dependence of each phonon scattering process and the other effects on the thermal conductivity except heat conduction by phonons:

$$\lambda_s = \lambda_0 K\left[\theta_1 \tan^{-1}(1/\theta_1) - \theta_2 \tan^{-1}(1/\theta_2)\right] + CT^3, \tag{4}$$

where λ_0 is the thermal conductivity of undoped UO_2 [19]; K, θ_1 and θ_2, the phonon scattering parameters which express the degrees of phonon scattering by point defects and extended defects [19]; C, a coefficient which express effects other than thermal conductivity by phonons [19]; and T, the temperature.

Figs. 5–8 compares the values calculated using Eq. (4) with those measured in this study. The measured values agree with the calculated data successfully below 1700 K. Above 1700 K, experimental data are slightly lower than the expected values. This decrease in thermal conductivity can be explained by the porosity change during experiments [17].

4.2. Burnup dependence on the thermal conductivity of irradiated fuel pellet

The measured thermal conductivities were normalized to the values of 96.5% TD (TD: theoretical density) by using the Loeb's equation:

$$\lambda_n = \lambda_m(1 - 0.035\varepsilon)/(1 - \varepsilon P), \tag{5}$$

where λ_n, the thermal conductivity normalized to that of 96.5% TD; λ_m, the measured thermal conductivity; ε, the parameter which express the effect of pore shape on the thermal conductivity of pellets; and P, the porosity evaluated from the sample density. The parameter ε is expressed as follows [30]:

$$\varepsilon = 2.6 - 5 \times 10^{-4}(T(K) - 273.15). \tag{6}$$

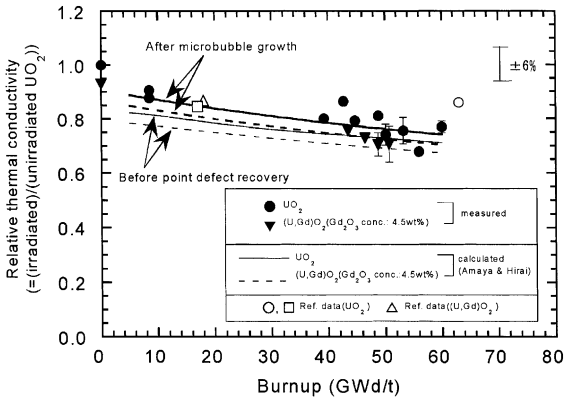

Fig. 10. Burnup dependence of relative thermal conductivity for irradiated fuel pellets at 1273 K. ●, ▼: measured values; ○, △, □: literature data [12,31,32]; ●, ○, □: UO_2; ▼: $(U, Gd)O_2$ (Gd_2O_3 concentration: 4.5 wt%); △: $(U, Gd)O_2$ (Gd_2O_3 concentration: 6 wt%) —: calculated by using Eq. (4) for UO_2; - - - - -: calculated by using Eq. (4) for $(U, Gd)O_2$ (Gd_2O_3 concentration: 4.5 wt%).

It was evaluated that the relative thermal conductivities for all irradiated samples of this study to those of unirradiated UO_2 pellets. Fig. 10 summarizes the relative thermal conductivities of irradiated UO_2 and $(U, Gd)O_2$ pellets at 1273 K, which are nearly the average temperature of the fuel pellets during irradiation. Data obtained by other researchers [12,31,32] are also shown for comparison. As shown in Fig. 10, the relative thermal conductivities of irradiated fuel pellets decrease with increasing burnups, but it seems that the relative thermal conductivities gradually saturate. The difference of the relative thermal conductivity between irradiated UO_2 and $(U, Gd)O_2$ pellets tends to become insignificant with increasing burnups. This suggests that the effects of soluble FPs and irradiation-induced defects on the thermal conductivity are larger than those of Gd_2O_3 in high-burnup fuel pellets.

The values calculated by using Eq. (4) agree well with the measured data and the data obtained by other researchers.

5. Conclusion

Thermal diffusivity was measured from room temperature to 2000 K by a laser flash method for microsamples prepared from UO_2 and $(U, Gd)O_2$ pellets irradiated in a commercial reactor. Their thermal conductivities were evaluated by multiplying the thermal diffusivities by the specific heat capacities of unirradiated UO_2 pellets and sample densities.

Thermal conductivities decreased with increasing burnup at lower temperature, then began to recover above about 800 K, and recovered completely above about 1500 K, becoming quite similar to the values for SIMFUEL (SIMulated high-burnup FUEL). The thermal conductivities of irradiated UO_2 and $(U, Gd)O_2$ pellets were analyzed based on the results of X-ray diffraction and TEM observations. The recovery stages of thermal conductivity corresponded with those of the irradiation-induced defects. Good predictions were made using the thermal conductivity expression of Amaya and Hirai, considering the effects of irradiation-induced defects.

Acknowledgements

This study was sponsored by the Ministry of Economy, Trade and Industry (METI).

References

[1] K. Nogita, K. Une, J. Nucl. Sci. Technol. 30 (1993) 900.
[2] K. Nogita, K. Une, Nucl. Inst. Meth. Phys. Res. B 91 (1994) 301.
[3] S. Kashibe, K. Une, K. Nogita, J. Nucl. Mater. 206 (1993) 22.
[4] Thermal conductivity of uranium dioxide, Technical Report Series No. 59, IAEA, Vienna, 1966.
[5] A.M. Ross, AECL-1096, CRFD-817, 1960.
[6] J.L. Daniel, J. Matolich, Jr., H.W. Deem, HW-69945, 1962.
[7] R.C. Hawkings, J.A.L. Robertson, AECL-1733, CRDC-1143, 1963.
[8] D.J. Clough, J.B. Sayers, AERE-R 4690, 1964.
[9] J.P. Stora, B. de Sigoyer, R. Deimas, P. Deschamps, B. Lavand, C. Ringot, CEA-R-2586, 1964.
[10] R.C. Daniel, I. Cohen, WAPD-246, 1964.
[11] H. Marchandise, EUR-4568f, 1970.
[12] J. Nakamura, M. Uchida, H. Uetsuka, T. Furuta, in: IAEA-TECDOC-1036, IAEA, Vienna, August 1998, p. 127.
[13] T. Namekawa, T. Mitsugi, T. Tachibana, S. Yamanouchi, in: Proceedings of the 35th Conference Remote Systems Technology, 1987, p. 105.
[14] K. Yamamoto, T. Hirosawa, K. Yoshikawa, K. Morozumi, S. Nomura, J. Nucl. Mater. 204 (1993) 85.
[15] S. Ishimoto, M. Hirai, K. Ito, Y. Korei, J. Nucl. Sci. Technol. 31 (1994) 796.
[16] P.G. Lucuta, Hj. Matzke, R.A. Verrall, H.A. Tasman, J. Nucl. Mater. 188 (1992) 198.
[17] M. Hirai, M. Amaya, Y. Wakashima, T. Matsuura, T. Nomata, H. Hayashi, M. Kitamura, in: IAEA-TECDOC-1036, IAEA, Vienna, August 1998, p. 139.
[18] M. Amaya, M. Hirai, Y. Wakashima, T. Kubo, T. Kogai, H. Hayashi, M. Kitamura, in: Proceedings of the TOPFUEL '97, BNES, June 9–12, Manchester, UK, 1997, p. 5.
[19] M. Amaya, M. Hirai, J. Nucl. Mater. 247 (1997) 76.

[20] T. Azumi, Y. Takahashi, Rev. Sci. Instrum. 52 (1981) 1411.
[21] Y. Takahashi, I. Yamamoto, T. Ohsato, Netsu-Sokutei 15 (1988) 103.
[22] D.L. Hagrman, G.A. Reyman (Eds.), TREE-NUREG-CR-0497, 1979.
[23] M. Hirai, J. Nucl. Mater. 173 (1990) 247.
[24] M. Rohde, B. Schultz, J. Nucl. Mater. 173 (1990) 289.
[25] J.C. Corelli, J. Hoole, J. Lazzaro, C.W. Lee, J. Am. Ceram. Soc. 66 (1983) 529.
[26] R.J. Price, J. Nucl. Mater. 46 (1973) 268.
[27] P.G. Klemens, Proc. Phys. Soc. A 68 (1955) 1113.
[28] P.G. Klemens, Phys. Rev. 119 (1960) 507.
[29] P.G. Klemens, G.F. Hurley, F.W. Clinard Jr., in: Proceedings of the 2nd Top. Mtg. Tech. Controlled Nuclear Fusion, American Nuclear Society, ERDA, EPRI, Conf-760935, 1976, p. 957.
[30] R. Brandt, G. Neuer, J. Non-Equilib. Thermodyn. 1 (1976) 3.
[31] J. Nakamura, K. Kamoshida, H. Nagashima, I. Owada, H. Uetsuka, in: Proceedings of the 2000 Spring Mtg. Atomic Energy Society Japan, 2000, p. K40.
[32] K. Minato, T. Shiratori, H. Serizawa, K. Hayashi, K. Une, K. Nogita, M. Hirai, M. Amaya, J. Nucl. Mater. 288 (2001) 57.